Supporting Information

for

Broadband sensitization of lanthanide emission with indium phosphide quantum dots for visible to NIR downshifting

Joseph K. Swabeck[1,2], Stefan Fischer[1,2], Noah D. Bronstein[1,2], and A. Paul Alivisatos[1,2,3,4,*]

[1]Materials Sciences Division, Lawrence Berkeley National Laboratory, Berkeley, California 94720, USA

[2]Department of Chemistry, University of California—Berkeley, Berkeley, California 94720, USA

[3]Department of Materials Science and Engineering, University of California—Berkeley, Berkeley, California 94720, USA

[4]Kavli Energy NanoScience Institute, Berkeley, California 94720, USA

Characterization

TRANSMISSION ELECTRON MICROSCOPY (TEM)

Low resolution TEM imaging was performed on a FEI Tecnai T20 S-TWIN TEM operating at 200kV with a LaB_6 filament. Images were collected with a Gatan Orius SC200.

High-resolution TEM (HRTEM) and scanning transmission electron microscopy (STEM) images were taken on a JEOL 2100-F microscope operating at 200 kV with a field emission gun.

STEM-EDS elemental maps were conducted on an FEI Titan 80-300 kV microscope operated at 200 kV with a probe current of 600 nA at the National Center for Electron Microscopy, Molecular Foundry, Lawrence Berkeley National Laboratory (LBNL). The STEM images were acquired using a Fischione high-angle annular dark-field (HAADF) detector with an inner semi-angle of 59 mrad. The EDS detector was an FEI Super-X Quad windowless detector operating with a solid angle of detection of 0.7 steradians. Bruker Esprit software was used for quantitative analysis.

POWDER X-RAY DIFFRACTION

Powder diffraction patterns of nanocrystalline samples were obtained using a Bruker D-8 GADDS diffractometer equipped with a Co Kα source.

ABSORBANCE

Steady state absorbance spectra were acquired with a Shimadzu UV-3600 double beam spectrometer operating with 1 nm slits at the second slowest setting.

FLUORESCENCE

Steady state fluorescence measurements were taken on two instruments. The first was a home built integrating sphere spectrophotometer. Details of the precise nature of the setup can be found in Bronstein *et al.*[1], but a brief description is as follows. A Fianium SC450 supercontinuum pulsed laser provided a white light source with an average illumination intensity

of 4 W from 410 nm to 2500 nm. The precise excitation wavelength was selected by passing the beam through two monochromators, a Princeton Instruments SP150 and a Princeton Instruments SP275. After wavelength selection was performed, the beam was sent through a beamsplitter to a calibrated photodiode to constantly measure the power of the beam, and the majority of the light was directed into the 25-mm entrance port of a 135 mm Spectralon integrating sphere from LabSphere. The sample was held using a custom built Spectralon circular cuvette holder on the opposite side of the sphere from the excitation. In addition to the tunable source, a second single wavelength laser was positioned to bypass the monochromators and enter thru the same port of the integrating sphere. The second laser was a Power Technology LDCU 12/6692 laser that emitted at 440 nm with a max power of 16 mW. The second laser was also passed through a beamsplitter to a photodiode to monitor the power. PLQY values used in the paper used an excitation power of 9.7 mW over ~1 mm^2 and were calculated by integrating the counts of the NIR Yb emission then comparing that value to the absorbed light at 440 nm. Direct reflections were blocked from exiting the sphere by a baffle, ensuring only diffuse light escaped the integrating sphere. The light exiting the sphere was focused onto the entrance slit of a Princeton Instruments SP2300 monochromator with a 300 g/mm grating blazed at 500 nm. The resultant spectrum was detected with either a Princeton Instruments PIXIS 400 B thermoelectrically cooled (TE) silicon CCD or an Andor iDus InGaAs (1.7 μm) camera. The CCD had been corrected for both spectral position using a Ne lamp and for sensitivity using a NIST-traceable radiometric calibration lamp from Ocean Optics, model HL3-plus, serial number 089440003.

The second setup that was used was an Edinburgh Instruments FLS980 equipped with a 450 W Xe-lamp and a single monochromator with two holographic gratings; 1800 g/mm blazed at 250 nm and 1200 g/mm blazed at 750 nm as an excitation source. The detection monochromator had three gratings; 1800 g/mm blazed at 500 nm, 1200 g/mm blazed at 750 nm, and 830 g/mm blazed at 1200 nm. Two photomultiplier tubes manufactured by Hamamatsu were attached, but only the TE-cooled R2658P with a spectral range of 200-1010 nm and a detector response of 800 ps was used. The system was calibrated for sensitivity by Edinburg Instruments.

EXCITATION SCANS

The excitation scans were performed on the aforementioned Edinburg Instruments FLS980. The method of making one of these PLE scans is shown in Figure S1. The detector was centered at 976 nm with a bandwidth of 10 nm. The excitation was scanned from 400-800 nm in 1 nm intervals, and the integrated intensity of the 976 nm centered emission was collected. This line was then compared against the absorptance (linear scale) of the sample, which is found by the following relation with the absorption (log scale).

$$Absorptance = 1 - 10^{-Absorption}$$

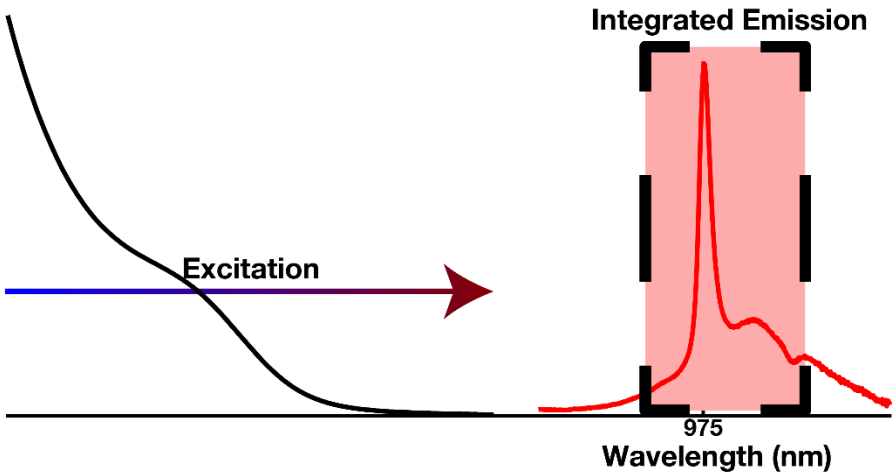

Figure S1. Cartoon schematic of the PLE measurement. The detection is kept constant while the excitation is scanned across the absorption.

The two lines were then normalized to the first excition peak and plotted against each other.

TIME RESOLVED FLUORESCENCE

For the time resolved photoluminescence (TRPL) measurements for the band edge of the InP QDs were taken on a PicoQuant Fluotime 300 with a PMA 175 detector and a LDH-P-C-405 diode laser with an excitation wavelength of 407.1 nm. The laser is capable of repetition rates of up to 80 MHz, but lower rates were used as appropriate to observe the full decay.

TRPL measurements of the NIR lifetimes of Yb were taken on the aforementioned Edinburgh FLS980. The excitation source that was used was an Nd:YAG pumped optical parametric oscillator, the Opolette HE 355 LD from Opotek. The laser covers a wavelength range of 410 to 2200 nm with a laser pulse length of ~7 ns and a repetition rate of up to 20 Hz.

EXAFS MEASUREMENTS

Extended x-ray absorption fine structure (EXAFS) measurements were taken on beamline 10.3.2 of the Advanced Light Source (ALS) at LBNL. This beamline was equipped with a bending magnet capable of producing x-rays from 2.1-17 keV in energy, and the ALS storage ring operates at 500 mA and 1.9 GeV. Samples were precipitated from solution, and the solid pellet was trapped in a piece of Kapton tape. The samples were then placed into the experimental apparatus and the signal was detected via the x-ray fluorescence of the samples. The XANES/EXAFS spectra were taken from 8845 to 9946 eV. Data analysis was first performed using the beamline's own processing software to correct any energy drift, deadtime, or glitching. The data was then processed using Artemis and Athena.[2]

Discussion of the Oxygenation of InP QD's

The surface of the native InP QD's is of utmost importance to the ability of the Ln ions to adhere to the QD's. Before the core/shell/shell geometry of the present dots was made, attempts to incorporate Ln ions into the lattice of InP QD's was attempted. These efforts were not

successful, probably due to the unfavorability of Yb incorporation into InP, but it was discovered that the Yb would adsorb onto the surface of the QD's. If optical measurements were taken immediately after they synthesis was completed, a moderate emission at 976 nm was observed, showing that the Yb ions were in some sort of contact with the QD's. If these particles were allowed to sit for a couple of days in an argon glovebox and the spectra were retaken, no luminesce was observed. This is presumably due to the desorption of the Ln ions from the surface of the QD.

Additionally, EXAFS measurements taken during this time period showed that the Yb ions of freshly prepared Yb decorated InP (InP:Yb) QD's showed that the Yb was exclusively coordinated by oxygen atoms. This was also true for samples made same day and loaded into the EXAFS tape in an argon glove box, so the oxygen around the Yb ions was not due to atmospheric contamination.

An argon purifier (NuPure Model E-200-CAG Eliminator) was added to the Schlenk line supply to try to remove the oxygen that we were seeing. The specifications of the purifier place the O_2 content at sub part per billion, orders of magnitude lower than argon straight from the cylinder (UHP, 99.9995%). This decrease in the oxygen content of the reaction resulted in InP:Yb QD's with no NIR emission, though the rest of the synthesis remained unchanged from before. This further confirmed that the surface of the native InP QD's had a significant oxygen layer on it.

In addition to being unable to affix the Ln ions to the surface of the InP QD's after the implementation of the argon purifier, the properties of standard syntheses of InP without any Yb changed as well. It was found that the PLQY of oxygen free InP QD's was much lower than that of QD's that were synthesized under UHP argon (<0.1% vs up to 5%). This would suggest that most InP QD's have a shell of In_2O_3 that passivates the surface and significantly changes the optical properties of the QD's. This has not been well explored, and seeing the size of the effect, it is something that deserves further study.

Table of Comparison with Previous Work

Material	Broadband Absorption	Absorption Coefficient	PLQY	Stability	Emission Width	Toxicity
$PbIn_2S_4$[3]	Yes (intrinsic bandgap ~1.4 eV)	~10^5 / cm	~5%	Medium	~25 nm	High (Pb)
$CsPbCl_3$[4]	Limited to UV-Blue	~10^5 / cm	~170%	Very Low	~25 nm	High (Pb)
YbF_3[5]	No (limited to the transition itself)	~ 22 / cm	~0	High	~5 nm	Low (insoluble)
Organic Dye-Yb couple[6]	Limited to UV-Blue	~10^3 / cm	~75%	Medium	~50 nm	Unknown
InP/$Yb_xY_{1-x}F_3$/LuF_3	Yes (intrinsic bandgap ~1.3 eV)	~10^5 / cm	~0.5%	High	~5 nm	Low (insoluble)

Table S1. Comparison of the current work with previous QD and dye based Yb sensitization schemes.

Additional TEM Characterization

STEM Contrast Curve Determination

In order to produce main text Figure 2b, 86 nanocrystals were analyzed using ImageJ as follows: lines were drawn from opposing corners of the nanocrystal to each other, and the intersection point of those lines was used as the center (Figure S2a). The center point of each particle was saved into a list, where they were used as the center of a radial integration. To do this, a circle is drawn around the central point, and the contrast value of the image along that surface is summed, creating a value for the contrast intensity at that distance from the center. This is shown schematically on Figure S2 with differently colored concentric rings, with warmer colors being later circles. The plot shows a cartoon of what the integrated intensity value would be at each point. One can see that in the left example, by the third circle the contrast is at its most extreme, so it would have an integrated value of 1. Since the contrast does not increase by the final ring, it would also be at 1. This is in contrast to the right example, where the particle is not perfectly symmetrical. In this case, the largest ring of the radial integration exceeds the size of the particle. In this instance, the integrated intensity of that ring would be lower than the one before, since it now has the low contrast background contributing to the total value (Figure S2b).

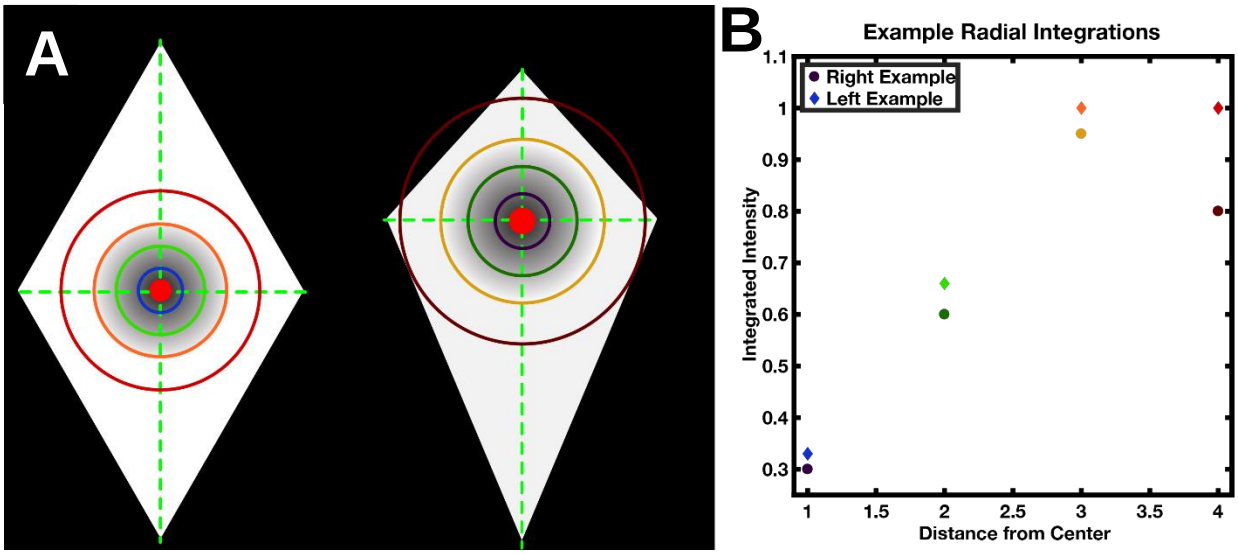

Figure S2. (a) Cartoon schematic of the process of radially integrating the contrast. The green lines on the left part of the figure show the process by which the center of the particle is determined, with the red dot being the found center. (b) From that found center, radial integration rings are shown, going from cool to warm colors. A representation of what the integrated intensities would be is shown at right as a graph.

By repeating this process many times, a number of curves are generated, from which we extracted an average and standard deviation, which are shown as Figure 2b in the main text.

STEM Contrast Simulation

Since contrast in HAADF-STEM goes as the atomic number squared (Z^2), we simulated the expected contrast of our HAADF images using the following method. The thickness of the

core/shell/shell nanoparticles was determined by looking at side stacked plates and was confirmed via a Scherer analysis of the relevant XRD reflections. The size of the InP core was determined by optical spectroscopy, using the first exciton energy to determine the size. In this experiment, the plates were determined to be 4 nm tall, while the InP cores were found to be 3.7 nm in diameter. Using the d-spacing for InP and LuF_3, this gives a total of, on average, 6.5 unit cells of InP at the center of the particles, with ~1 unit cell of LuF_3 on it. The shell of the particle is then found in the same way to be ~9 unit cells of LuF_3. We then used the following equations to determine the contrast.

$$Z_{shell} = 71$$

$$Z_{core} = \frac{6.5}{7.5} \times 49 + \frac{1}{7.5} \times 71$$

$$Contrast\ Ratio = \frac{{Z_{core}}^2 \times 7.5}{{Z_{shell}}^2 \times 9} = \frac{20228}{45369} = 0.45$$

This gives a contrast value well within error of what is observed in main text Figure 2b.

FOURIER FILTERING OF HRTEM

The HRTEM image shown in main text Figure 2c was further analyzed via Fourier filtering. To do this, the image was converted into Fourier space via the FFT function of Gatan Digital Micrograph (Figure S3a). This FFT shows two different lattice domains, highlighted in green and blue. By applying a filter where the highlights are, we were able to decompose the image into its constituent lattices.

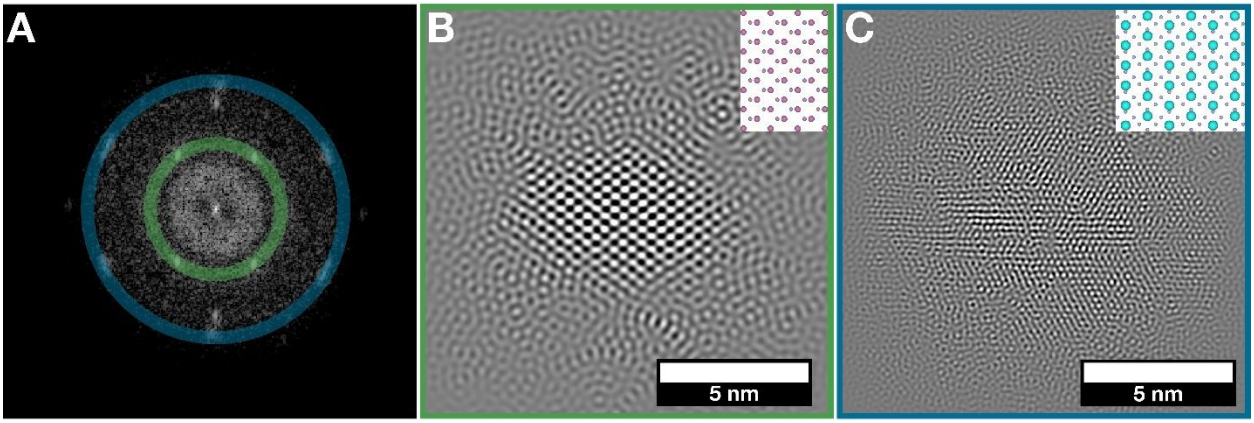

Figure S3. Fourier filtering of main text Figure 2c. (a) The FFT of the initial image, showing the two different lattice spacings. (b) and (c) Color coded inverse FFT's taken from the regions in (a).

In Figure S3b, the core of the nanocrystal that had been highlighted by the green field in 3a is clearly seen. This shows the [110] plane of InP, and it confirms that the InP is at the core of the core/shell/shell system. Looking at the inverse FFT of the blue region, the [001] lattice of LuF_3 is seen with its expected lattice spacing.

This kind of alignment of the core of the nanocrystal with the shell in the TEM was rare, but in the two particles it was observed in, the InP [110] was consistently ~30° offset from the LuF_3 [001]. Since there were not many particles observed this way, no conclusion can be drawn from

the orientation angles, but this kind of study could provide insight into how these two different materials grow on each other.

SIDE VIEW OF CORE/SHELL/SHELL PLATES

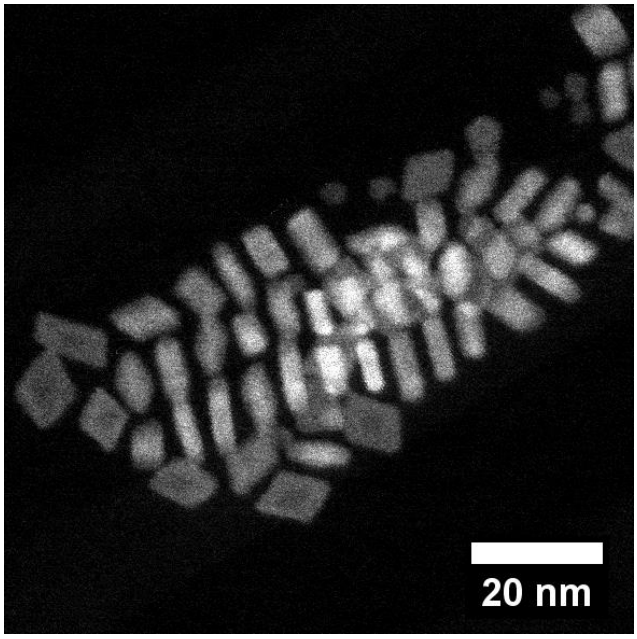

Figure S4. This side on STEM image shows the core/shell/shell nanocrystals to be ~4 nm in height. Note that this sample did not have a rigorous size selection applied to it, resulting in the other morphologies (namely, dots) that are seen.

EDS MAPS OF CORE/SHELL/SHELL NANOCRYSTALS

Elemental maps of the core/shell/shell nanocrystals were taken to help determine the stoichiometry and structure of the crystals.

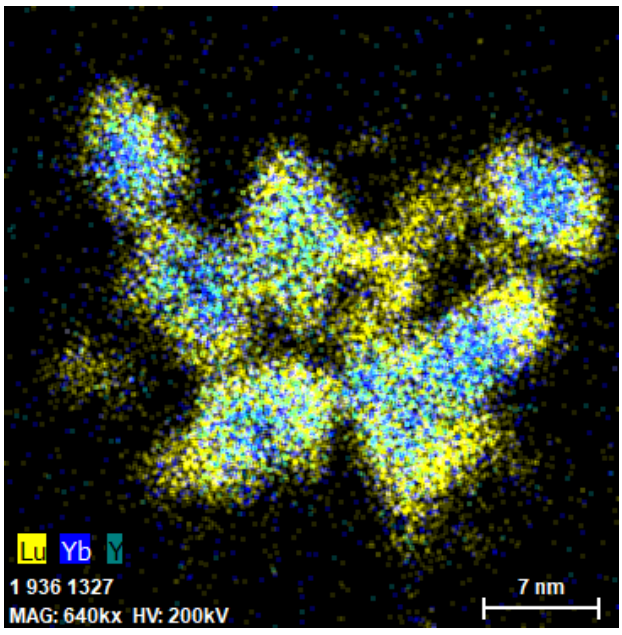

Figure S5. STEM-EDS image of core/shell/shell nanocrystals. The presence of Y and Yb in the core of the nanocrystal is confirmed, as is the Lu rich nature of the shell.

In all of the EDS maps that were taken of the nanocrystals, the In and P components of the nanocrystals were difficult to detect. For the In, EDS maps localized it to the nanocrystals, but were too low signal to determine if it was in the core or the shell. The P peak appeared on the shoulder of the much stronger Y peak, which was difficult to deconvolute. For the elements that we were able to resolve, Table S2 shows the elemental percentages, as taken from ~15 particles.

Atom %	Core	Shell
Lu	0.28	0.36
Yb	0.39	0.31
Y	0.46	0.29

Table S2. Rare earth distributions as determined by STEM EDS.

XRD CHARACTERIZATION

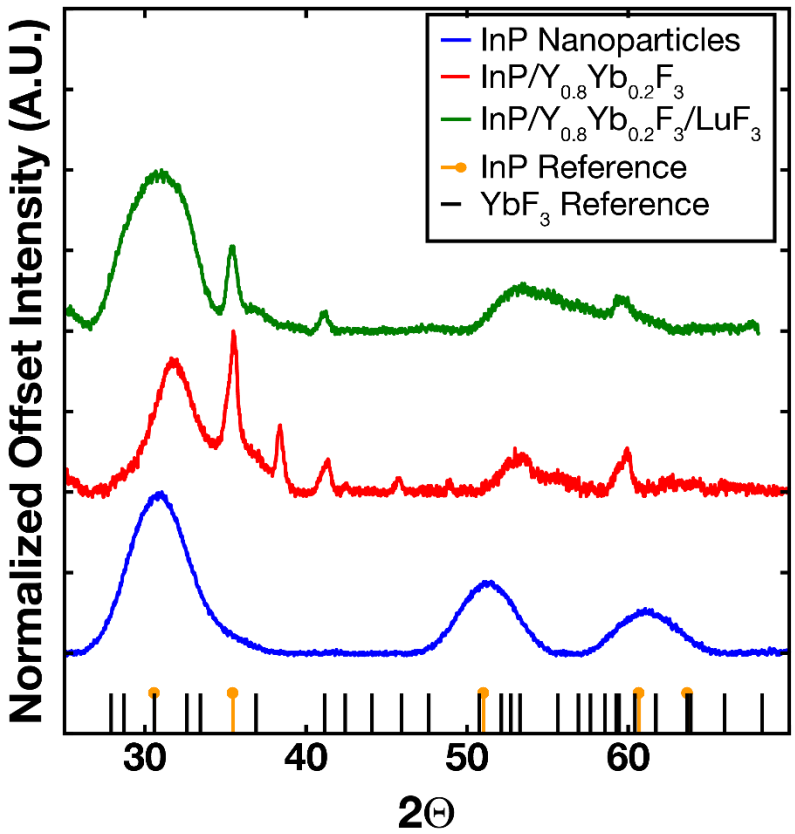

Figure S6. XRD spectra of the core (blue), core/shell (red), and core/shell/shell (green) nanoparticles. The references are to cubic InP (PDF number 01-073-1983) and orthorhombic YbF_3 (PDF number 01-071-1161). The reference for LuF_3 was unavailable, so YbF_3 shows roughly where the peaks should be found. Note that the LuF_3 reflections that correspond to the

lateral dimension of the nanoplates are sharp, while those that correspond with the height of the plate are broadened.

EXAFS Parameters and Fits

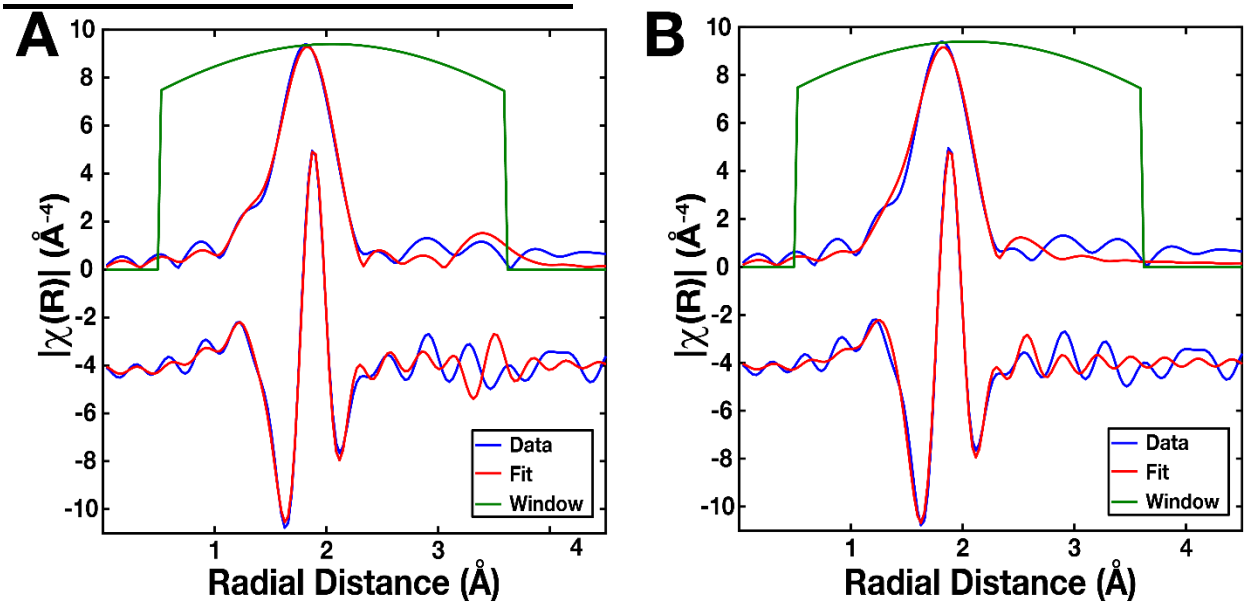

Figure S7. Comparison of the EXAFS fit of YbF_3 (a) and YbOF (b). Part (a) is also main text Figure 3b.

The difference between the two fits is somewhat subtle, but Table S3 shows that the fluoride fit is much better than the oxy-fluoride fit, evidenced by the much lower R-factor and reduced chi squared.

Sample	YbF_3	YbOF
Independent Points	10.56	10.56
Number of Variables	7	7
$\chi 2$	2549.16	5273.80
Reduced $\chi 2$	716.34	1481.99
R-Factor	0.0122	0.0245
k-range (Δk)	2-10 (1)	2-10 (1)
R-range (ΔR)	1-3.1 (1)	1-3.1 (1)
Window Type	Kaiser-Bessel	Kaiser-Bessel

Table S3. Data regarding the EXAFS fits performed. Identical numbers of parameters were used to perform the two fits, as not to bias the results.

YbF_3	N	$S0_2$	s^2	E_0	ΔR	R_{eff}	R
F2.1	2	1.129	0.0023	0.653	0.03414	2.2341	2.26824
F1.1	6	1.129	0.0145	0.653	-0.0584	2.2737	2.2153
F1.4	2	1.129	0	0.653	0.32986	3.5269	3.85676
F2.1 F 1.1	6	1.129	0.0084	0.653	-0.01213	3.5291	3.51697
YbOF							
O1.1	2	1.26	0	-0.579	0.06314	2.192	2.25514
O1.3	2	1.26	0	-0.579	-0.12093	2.2469	2.12597
F1.1	1	1.26	0.00731	-0.579	0.61822	2.2533	2.87152
F1.2	2	1.26	0	-0.579	-0.057	2.3516	2.2946

Table S4. Detailed parameters of the two different EXAFS fits. Note the non-physical Δr values in the YbOF fit.

Additional Optical Data

Native And Treated InP Optical Spectra

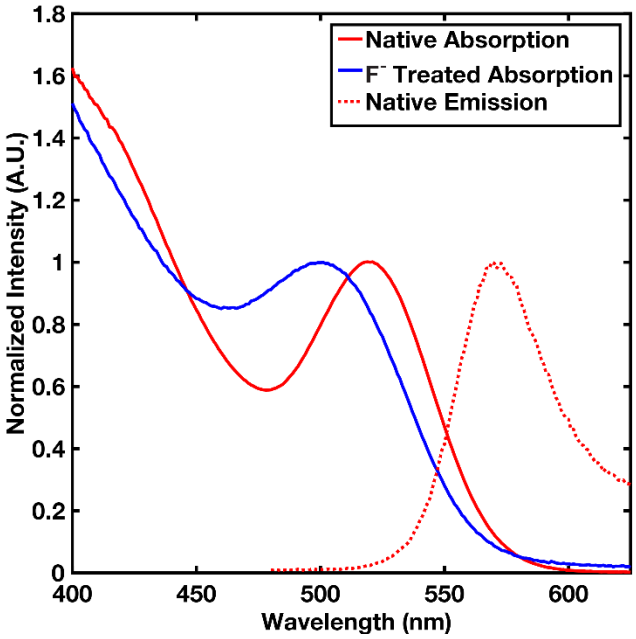

Figure S8. Comparison of the native InP QD absorption with that of the F^- treated InP. The PL of the native InP shows the start of some small oxide trap state emission on the red end of the spectrum due to the rapid oxidation of InP upon removal from the glovebox. The PL of the fluoride treated QD's is shown in Figure S11, and it does not show that same trap emission.

Absorption of all Materials Used

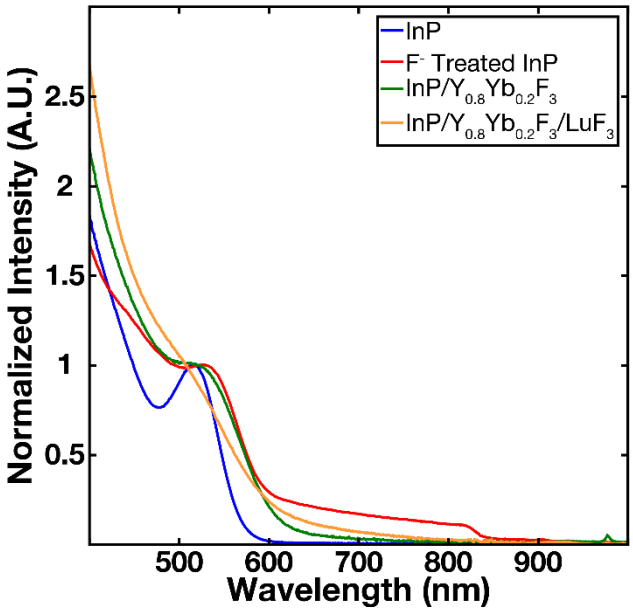

Figure S9. Comparison of the absorption spectra of all steps. The ~830 nm feature of the F^- treated InP is due to a combination of detector switchover and scattering, as the treated quantum dots do not have good colloidal stability. Note the lack of a NIR absorption.

Luminescence Properties Under Different Excitation Conditions

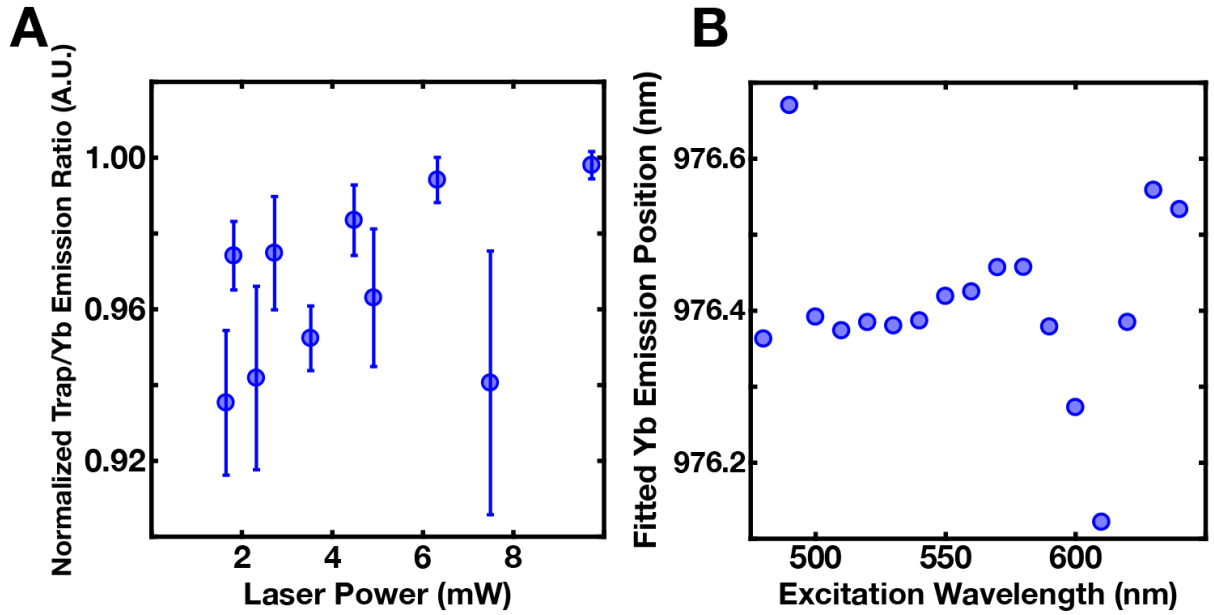

Figure S10. (a) Normalized ratio of the trap emission of InP/$Y_{0.8}Yb_{0.2}F_3$/LuF_3 to the NIR Yb emission under varying laser intensities. The excitation wavelength was constant at 440 nm and a series of neutral density filters were used to decrease the laser power. There is no clear trend within error, showing that the optical performance of the system is insensitive to the excitation power. (b) Peak wavelength of the NIR Yb emission (as determined via a Gaussian fitting of the top half of the peak) vs the excitation wavelength. There appears to be no correlation between the excitation wavelength and the emission wavelength, again showing the robust nature of the Yb emission.

Band Edge and NIR Luminescence of Yb Free Nanocrystals

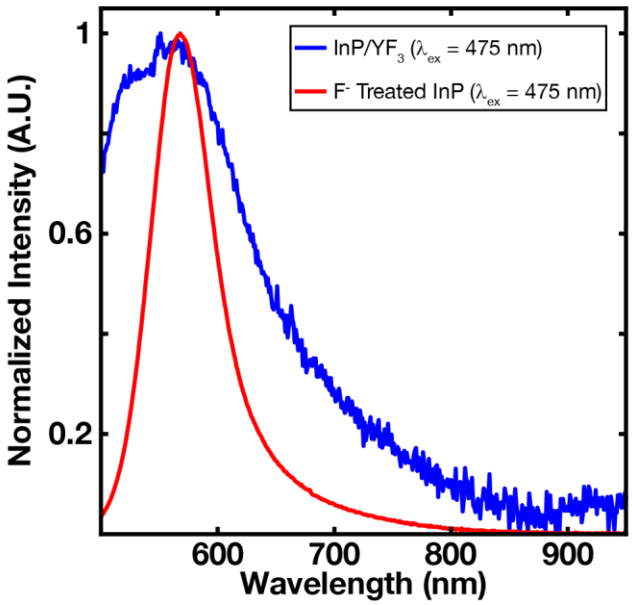

Figure S11. PL spectra of undoped nanoparticles. The red curve shows the luminescence of fluoride treated InP before any rare earth shelling steps were taken, while the blue curve shows the weak luminescence of InP/YF_3 nanocrystals. In both cases, note the lack of the trap emission that is seen in the Yb containing nanoparticle systems.

FURTHER EXPLORATION OF MAIN TEXT FIGURE 4A

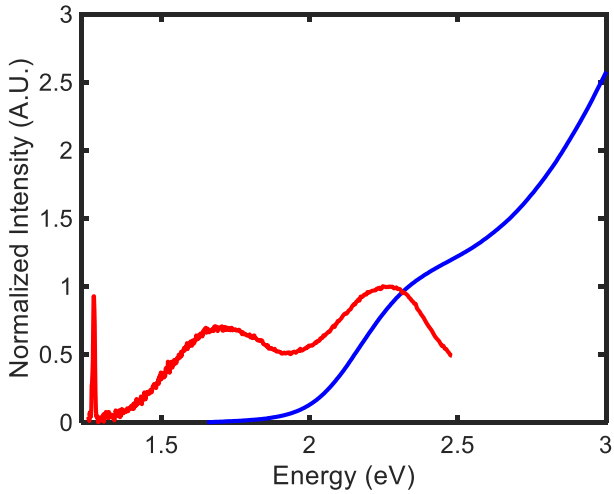

Figure S12. The PL (red) and absorption (blue) seen in main text Figure 4a plotted in energy space. Note that plotting in this way reveals that the trap and band edge emission features are similar in width, which suggests that the broadness of the trap comes from the many different sizes of InP QD.

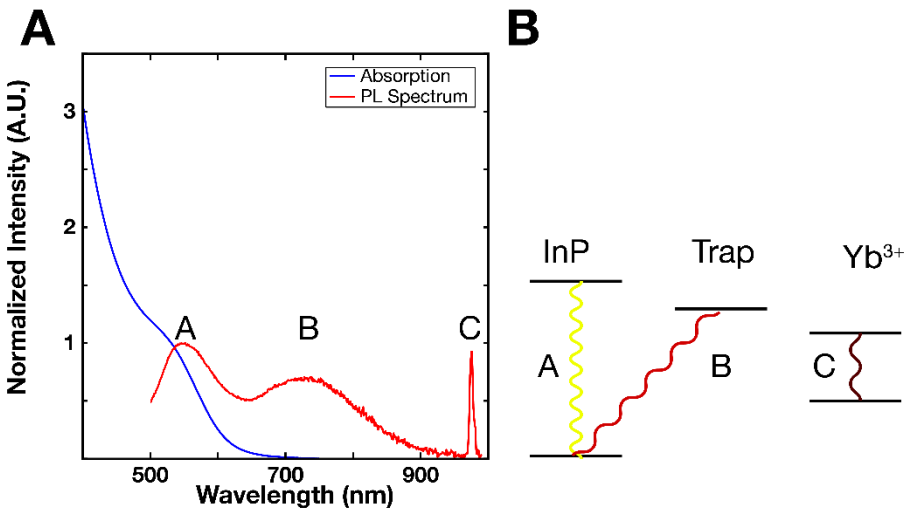

Figure S13. Cartoon of the states that lead to the emission spectrum seen if main text Figure 4a.

FULL LIFETIMES OF FIUGRE 4C

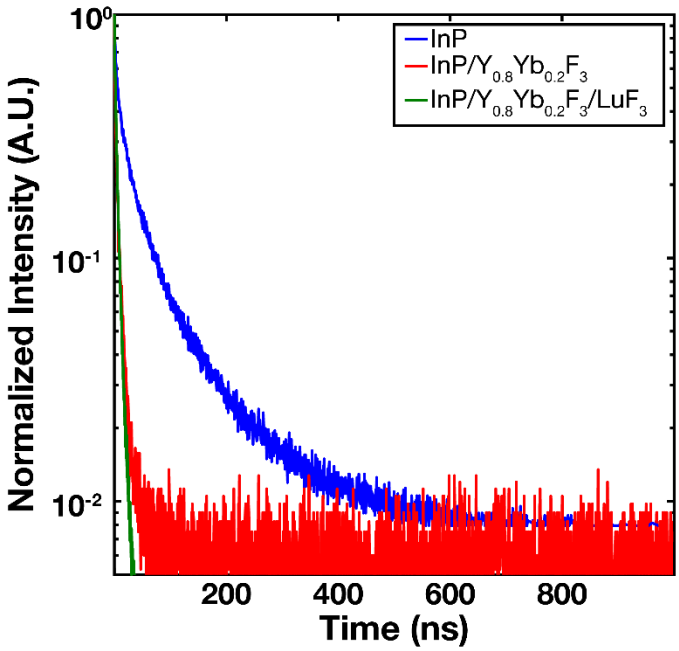

Figure S14. Full view of the lifetimes from main text Figure 4c.

NIR PL of Nd Doped Core/Shell/Shell Nanoparticles

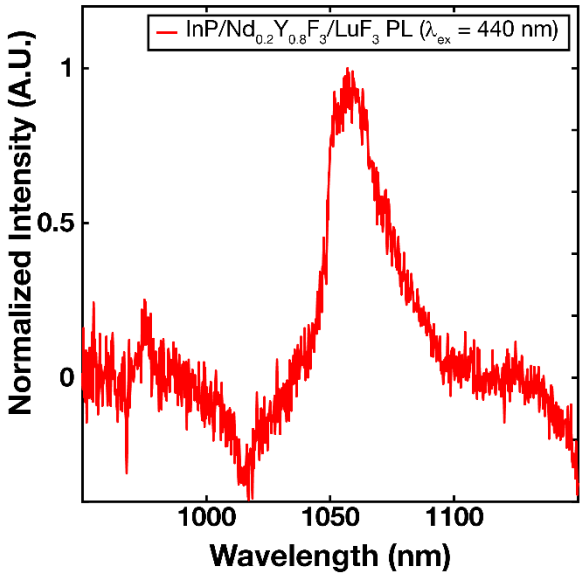

Figure S15. Photoluminescence curve of $InP/Nd_{0.2}Y_{0.8}F_3/LuF_3$ under 440 nm excitation showing the NIR emission of the $^4F_{3/2}$ -> $^4I_{11/2}$ transition. The dip in the PL just before the peak is due to the absorption of the solvent combined with the baselining of the emission.

Comparison of Band Edge and Trap Excitation

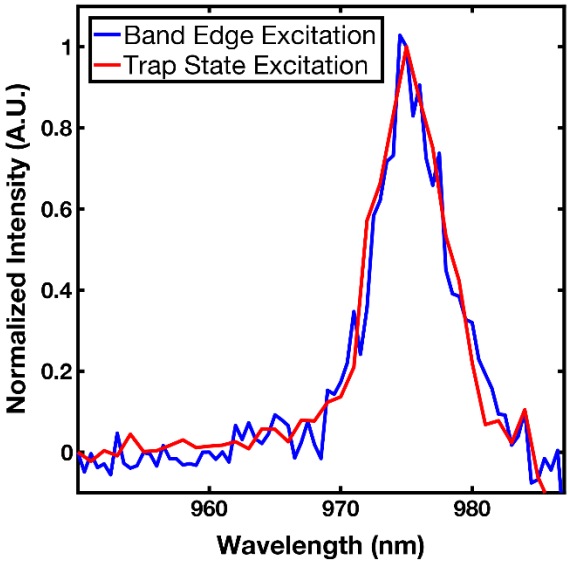

Figure S16. Photoluminescence curve of $InP/Yb_{0.2}Y_{0.8}F_3/LuF_3$ under two illumination wavelengths. The blue curve shows the PL that results from band edge excitation (λ_{ex} = 500 nm) while the red curve shows the PL from exciting the peak of the second feature in the PLE (see main text Figure 4b).

References

(1) Bronstein, N. D.; Yao, Y.; Xu, L.; O'Brien, E.; Powers, A. S.; Ferry, V. E.; Alivisatos, A. P.; Nuzzo, R. G. Quantum Dot Luminescent Concentrator Cavity Exhibiting 30-Fold Concentration. *ACS Photonics* **2015**, *2* (11), 1576–1583.

(2) Ravel, B.; Newville, M. ATHENA , ARTEMIS , HEPHAESTUS : Data Analysis for X-Ray Absorption Spectroscopy Using IFEFFIT. *J. Synchrotron Radiat.* **2005**, *12* (4), 537–541.

(3) Creutz, S. E.; Fainblat, R.; Kim, Y.; De Siena, M. C.; Gamelin, D. R. A Selective Cation Exchange Strategy for the Synthesis of Colloidal Yb3+-Doped Chalcogenide Nanocrystals with Strong Broadband Visible Absorption and Long-Lived Near-Infrared Emission. *J. Am. Chem. Soc.* **2017**, *139* (34), 11814–11824.

(4) Milstein, T. J.; Kroupa, D. M.; Gamelin, D. R. Picosecond Quantum Cutting Generates Photoluminescence Quantum Yields Over 100% in Ytterbium-Doped CsPbCl 3 Nanocrystals. *Nano Lett.* **2018**, acs.nanolett.8b01066.

(5) Ribeiro, C. T. M.; Zanatta, A. R.; Nunes, L. A. O.; Messaddeq, Y.; Aegerter, M. A. Optical Spectroscopy of Er3+ and Yb3+ Co-Doped Fluoroindate Glasses. *J. Appl. Phys.* **1998**, *83* (4), 2256–2260.

(6) Hu, J.-Y.; Ning, Y.; Meng, Y.-S.; Zhang, J.; Wu, Z.-Y.; Gao, S.; Zhang, J.-L. Highly near-IR Emissive Ytterbium(<scp>iii</scp>) Complexes with Unprecedented Quantum Yields. *Chem. Sci.* **2017**, *8* (4), 2702–2709.